PROCEEDINGS OF SPIE

SPIEDigitalLibrary.org/conference-proceedings-of-spie

Full-aperture optical metrology for inflatable membrane mirrors

Quach, Henry, Berkson, Joel, Sirsi, Siddhartha, Choi, Heejoo, Dominguez, Ruben, et al.

Henry Quach, Joel Berkson, Siddhartha Sirsi, Heejoo Choi, Ruben Dominguez, Brian Duffy, David Lesser, Yuzuru Takashima, Art Palisoc, Christopher Walker, Dae Wook Kim, "Full-aperture optical metrology for inflatable membrane mirrors," Proc. SPIE 11487, Optical Manufacturing and Testing XIII, 114870N (20 August 2020); doi: 10.1117/12.2569750

SPIE.

Event: SPIE Optical Engineering + Applications, 2020, Online Only

Full-Aperture Optical Metrology for Inflatable Membrane Mirrors

Henry Quach[a], Joel Berkson[a], Siddhartha Sirsi[a,b], Heejoo Choi[a,c], Ruben Dominguez[b], Brian Duffy[b], David Lesser[b], Yuzuru Takashima[a], Art Palisoc[d], Christopher Walker[a,b], Dae Wook Kim[a,b,c,*]

[a]Wyant College of Optical Sciences, University of Arizona, 1630 E. University Blvd., Tucson, AZ 85721, USA
[b]Department of Astronomy, University of Arizona, 933 N. Cherry Ave., Tucson, AZ 85721, USA
[c]Large Binocular Telescope Observatory, University of Arizona 933 N Cherry Avenue, Tucson, AZ 85721, USA
[d]L'Garde, Inc. 15181 Woodlawn Avenue, Tustin, CA 92780, USA

ABSTRACT

The ability of space telescopes to see into nascent protostellar systems and even further into our universe is driven by the size of their deployable light collection area. While large monolithic mirrors typically weigh tons, inflatable membrane mirrors present a scalable, ultralightweight alternative. Leveraging decades of advances in adaptive optics technology, the possibility of a well-corrected 20 meter-class space observatory such as the Orbiting Astronomical Satellite for Investigating Stellar Systems (OASIS) is strikingly feasible.

However, with great aperture size, comes great metrology requirements. Membrane reflectors are characteristically structured as one transparent and one metallized polymer membrane sealed around a steel tensioning ring. The inflated surface does not naturally conform to a known or prescribed conic but an approximate Hencky surface. Furthermore, multiple internal reflections and polarization interactions between the dielectric and metal layers disturb coherent light that probes it. A non-contact, full-aperture testing method is needed and further, one that can test highly varying membranes after thermoforming too.

We present our method in obtaining the absolute shape of thermally formed, inflatable reflectors for space telescopes. Our work measures a 1-meter prototype of the OASIS primary inflatable mirror. Evolving from laser distance scanning to photogrammetry to deflectometry, our survey of metrology techniques for inflatable membrane optics is discussed.

Keywords: Membrane Inflatable Mirrors, Space Telescopes, Hencky Surface, Photogrammetry, Deflectometry, Large Aperture Metrology

1. INTRODUCTION

1.1 OASIS – Science Goals and Objectives

The Orbiting Astronomical Satellite for Investigating Stellar Systems (OASIS) is a 20-meter class space observatory that will perform high spectral resolution observations at terahertz frequencies, shown in Figure 1. Over its nominal 2-year mission, OASIS will probe conditions and search for biogenic molecules (e.g., water) towards hundreds of protoplanatery disks and solar system objects.[1] With its large collecting area and suite of terahertz heterodyne receivers, OASIS will have the sensitivity to explore the role water plays in the formation and evolution of planetary systems. The science goals of OASIS are:

1) Understand the origin of the Earth's oceans.
2) Understand the source and mechanisms by which water outgasses from solar system objects.
3) Understand the role gas mass has in the evolution of proto-planetary systems.
4) Understand the role water plays in planet formation.
5) Understand the transport of water from the outer to inner solar system.

*letter2dwk@hotmail.com

Optical Manufacturing and Testing XIII, edited by Dae Wook Kim, Rolf Rascher,
Proc. of SPIE Vol. 11487, 114870N · © 2020 SPIE · CCC code:
0277-786X/20/$21 · doi: 10.1117/12.2569750

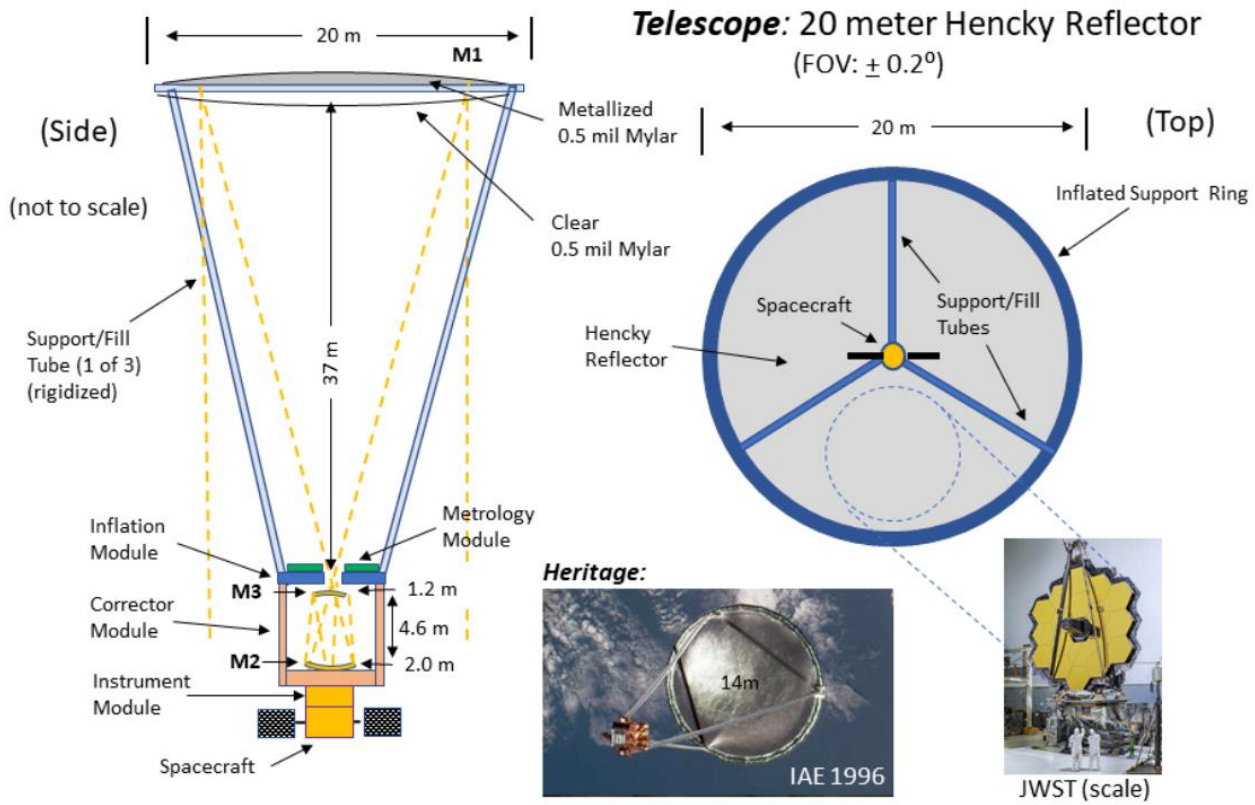

Figure 1. The telescope consists of an inflatable reflector secured to a spacecraft via deployable struts. The innovative structure allows packaging of a large aperture telescope within available launch volumes/masses. OASIS will have ~30x the collecting area and ~6x the angular resolution of Herschel and complements the short wavelength capabilities of JWST.

1.2 Background on Inflatable Optics

The Echo balloon project by NASA in the 1960's was the first successful demonstration of large-scale inflatable membranes, which were 30m diameter orbiting spheres constructed from metallized Mylar.[2] They operated as reflectors for radio waves between 162 to 2390 Mhz and successfully stayed in orbit for several years. Project Echo's success triggered multiple investigations into large scale membrane reflectors, including a 14-meter diameter paraboloid reflector deployed onboard STS-77 in the late 1990's. This experiment was termed as the inflatable antenna experiment (IAE) and demonstrated the on-orbit deployment of an inflatable membrane reflector.[3] While the deployed reflector attained the desired geometry, an underestimation of residual gas at packaging led to uncontrolled dynamics in the deployment process. In the early 2000's, research at the University of Arizona developed prototypes of stretched membranes with electrostatically induced curvature.[4] More stable architectures with low areal densities such as lenticular inflatables were also investigated and developed by L'GARDE and SRS technologies.[5] These mainly consisted of a primary membrane mirror supported by lenticular inflatable panels. Primary challenges observed were the persistence of uncontrolled frequency modes and lack of adequate shape control. Concurrently, Ball Aerospace's and DARPA's MOIRE program aims to place a GEO based 20-m diameter operational telescope for persistent monitoring of the ground on Earth.[6] Advances in transmissive diffractive optics techniques have greatly relaxed surface precision requirements from telescope mirrors.

Among surveyed membrane mirror technologies, it becomes evident that major technology areas need further development before a reliable meter scale membrane reflector can operate on orbit. From an optical standpoint, active wave-front control for manipulating shape of the optical signal would be necessary to bring down mirror surface accuracy requirements. This would allow larger tolerances on surface inaccuracies. From the structural standpoint, design emphasis must extend to include packaging and deployment geometries in addition to final desired shapes. A major constituent of space telescopes are peripheral supporting structures. They play an instrumental role in precise placement and alignment of membrane optics.

1.3 Shape of Pressurized Thin Membranes

In the absence of preforming, the deformed shape of a pressurized, isotropic circular membrane (or thin plate) is called a Hencky surface.[7] This name originates from the surface's 1D profile across any diameter, known as the Hencky curve and was first solved for by its namesake in 1915.[8] The 1D profile of the Hencky surface does not resemble a standard conic cross-section; rather, if the best fit parabola is subtracted from it, a 'W-curve' is characteristic. This has been shown across both analytic and FEM solutions. Meinel characterized the non-rotationally symmetric shape as the combination of excess spherical aberration and astigmatism.[9]

In practice, inflated membranes for space applications deviate from the theoretical Hencky surface because their materials have anisotropic mechanical properties. For example, Kapton and Mylar are commonly selected for spacecrafts due to their low outgassing, temperature stability, and radiation weathering resistance.[10] However, the manufacturing processes of either film requires an initial molten sheet to be pulled along a primary direction. The machine-pulled direction and the transverse directions produce distinct Young's moduli and yield stresses in Mylar.[11] Consequently, the surface height profile of the inflated membrane varies based on the azimuthal slice taken for observation. The biaxial nature of the resultant surface may be fit as a biconic freeform when analyzed in optical design software.

L'Garde wrote a code called FLATE that solves the *inverse problem*, obtaining surface accuracies on the order of a millimeter RMS for paraboloids. The problem can be stated: given known membrane material properties, what must be the initial uninflated shape such that a spherical or paraboloidal surface of revolution is obtained when inflated to the desired pressure? FLATE outputs not only this initial shape but also the gore flat pattern, which specifically accounts for greater reflector thickness at seams due to the tape and adhesives. Using shaped gores based on the desired film stress allows for choosing pressures that are high enough to achieve the desired wrinkle-free surface but low enough to not exceed the yield strength of the material.

1.4 Problem Statement: Metrology Selection

A general metrology technique must be able to capture surface shapes that are relatively unknown due to latent wrinkles and possible thermoforming variation. Beyond this dynamic range requirement, the technique must also obtain a global accuracy in the tens of microns range, as roughly estimated for basic terahertz imaging performance, $\lambda/8 = 67$ μm.

Early discussions adjourned interferometry as the primary candidate. Generating the breadth of null optics required to capture every possible inflated shape, even within a generous height envelope of tens of microns, is not financially accessible.

We also considered tactile solutions such as low-force contact profilometers for their large measurement range and micron scale sensitivity. However, profilometers require a motion travel range at least as large as the unit under test (UUT) and in this case, would require least 1m of travel across a Cartesian gantry. Since inflation pressure range is so low (P = 0.050-0.100 psig), appropriate tracking styluses with touch probe force in the mN range severely limit sampling speeds across the aperture. Unfortunately, the combined effects of contact probe tracking force, minimum motion gantry size, and required full aperture scanning time render this regime of solutions unideal as well.

In lieu of the traditional repertoire for precision metrology, our 1m diameter scale model of the OASIS primary assembly served as the primary UUT to assess other metrology candidates.

2. INFLATABLE MEMBRANE MIRROR PROTOTYPE AND CHARACTERIZATION

2.1 Surface Roughness Characterization of Membrane Materials

We obtained samples of aluminized Mylar sheet and aluminized Kapton sheet, courtesy of L'Garde Inc. Both 20" diameter samples were analyzed for surface roughness by a Zygo NewView 8300 white light interferometer, as summarized in Table 1. The Ra and RMS values imply that both foils are specularly reflective since the magnitude of surface height deviations is much less than the wavelength of visible light, $\lambda \approx 500$ nm. Note that the PV of both materials is in the tens of microns range.

A closeup in Figure 2 reveals that underlying phenomena were higher frequency small peaks and lower frequency pits distributed across the membrane. The specular nature of both sheets is apparent from a human glance, but the surface statistics provide quantitative metrics to guide metrology selection.

Table 1. Micro surface roughness of sampled areas. Here, Ra refers to the arithmetic mean of the absolute height values sampled across 834 μm x 834 μm areas. The RMS value refers to the root mean square of the surface values and PV is the difference between the two extreme height values in that same area. The tabulated statistics were calculated as the average of the individual surface statistics for the center, edge, and interior samples of the sheets.

Sample (thickness)	Ra (μm)	RMS (μm)	PV (μm)
Kapton (12.7 μm)	0.026 ± 0.001	0.043 ± 0.005	5.432 ± 2.576
Mylar (12.7 μm)	0.010 ± 0.002	0.019 ± 0.004	12.897 ± 4.164

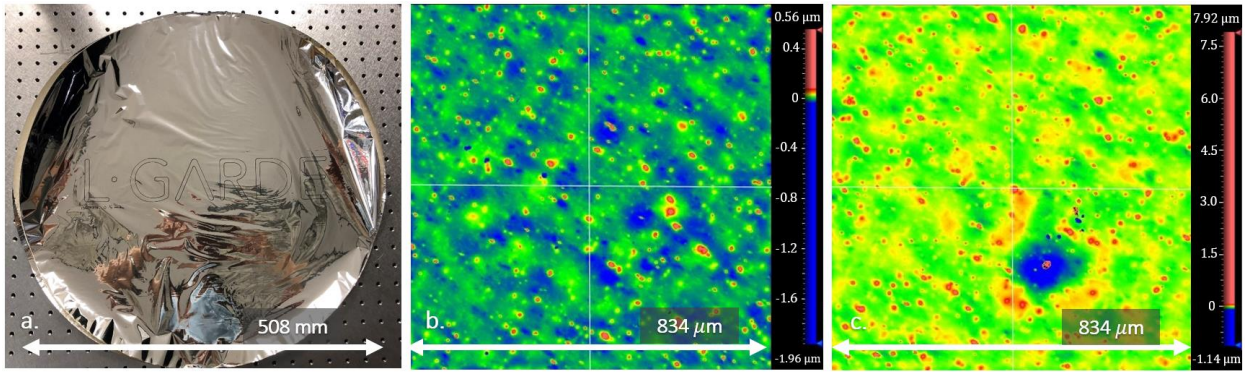

Figure 2. The 0.5 mil thick, 20" circular Mylar sample shows wrinkles across the aperture without applied tension, a. When pulled taut and analyzed by the white light interferometer, the surface reveals a PV of tens of microns, b. However, a closer inspection of the extrema shows that the large PV is due to random irregularities from the foil manufacturing process, such as aggregate metal dust. c. The presence of these defects challenge the dynamic range limits of coherent null techniques such as interferometry, but simply add some noise to incoherent image acquisitions by virtue of surface scattering.

2.2 OASIS Inflatable Primary Mirror Prototype

A 1m scaled down model of the primary was built by clamping one transparent mylar sheet in the front and one aluminized mylar sheet for the back optical surface between two machined rings with O-ring seals. Pressurizing the sealed membrane created a convex, transparent frontal surface and the concave, reflective rear surface of interest. To find the approximate focal length at several pressures, we began by masking the aperture to 100 mm. Masking reduces aberration caused by marginal rays at the outer rim so that best focus is more resolvable. Simple point-to-point conjugate imaging in a 4f imaging configuration was used to find both astigmatic foci. The focus locations are highlighted in Figure 3 and summarized in Table 2.

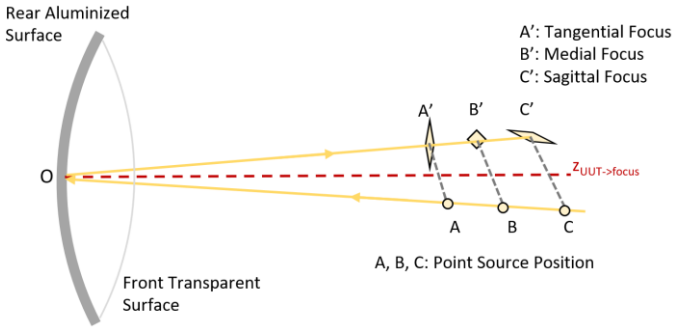

Figure 3. Focal length estimation was performed by using a small, highly luminous LED as a pseudo point source to illuminate the optic. This LED was affixed to a flat plate, which served as the image plane. The combined assembly was translated along the optical axis (red) until the sharpest vertical and horizontal lines were obtained, which indicate the tangential focus and sagittal focus positions, respectively. A commercial laser distance meter, accurate to 1 mm, measured the distance between the test assembly plane and membrane aperture plane. The medial focus position B' was calculated as the average of A' and C'. Lateral distances AA', BB', and CC' were measured to be ~3.5- 4 cm, which are small. Note that OA = OA', OB = OB', and OC = OC', because the point source and image plane were coplanar.

Table 2. Astigmatic focal lengths for several membrane inflation pressures. At the selected pressures, the optic is a relatively fast concave surface. Astigmatism is present without any pretreatment due to the orthotropy of the constituent 1 mil thick Mylar foils.

Pressure (psig)	Tangential Distance $d_{OA'}$ (mm)	Sagittal Distance $d_{OC'}$ (mm)	S-T Distance $d_{A'C'}$ (mm)	f_{medial} $d_{OB'}/2$ (mm)	f/#
0.050	4468	4803	335	2318	2.3
0.060	4215	4601	386	2204	2.2
0.100	3648	3930	282	1895	1.9

2.3 Wrinkle Characterization and Thermoforming Treatment

Laying and clamping the thin mylar sheet without uniform prestress results in wrinkles in several regions. Figure 4 shows reflected image of a checkerboard as distorted towards the aperture edge. Wrinkles are invariably extant but vanish at higher inflation pressures, where tensile stress is more uniform in all directions. However, they are undesirable at any pressure because they produce steep and varying surface slopes that limits the usable light-collecting aperture. Optimal performance of a large membrane primary requires maximal clear aperture as well as uniformity among all azimuthal profiles to minimize the medial spot size at best focus.

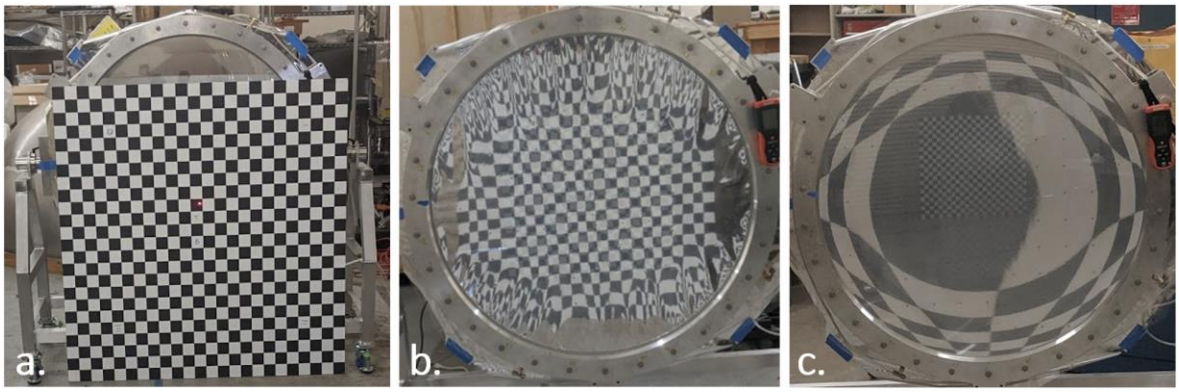

Figure 4. A large 48” x 48” checkerboard grid with 2” x 2” squares was placed 2.5m in front of the test assembly, with a camera capturing an image at that same distance. The scale of the checkerboard in relation to the mylar membrane is shown for comparison, a. When inflated to 0.020 psig, cobweb-like features manifests towards the aluminum ring edge, b. When inflated to 0.050 psig, the undulations of the web equilibrate into a smoother surface, c.

To survey the variety of realizable shapes at different inflation pressures, pretreatment process development is in order. Chandra posits that surface nonuniformities can be removed via controlled plastic deformation of the pressurized membrane.[12] If a surrounding fluid heats the membrane to its glass transition temperature, the wrinkles can be ironed out by the effect of molecular structural reorganization to favorably distribute stress across non-uniform regions.

2.4 LiDAR Point Scanning and Reverse Beam Footprint-based Mirror Shape Measurement

A number of non-contact diffuse point measurement techniques, including those used to test membrane optics, have been used to measure coarse shapes not generated by precision machining and polishing. Photogrammetry has been used measure diffuse meter-class solar concentrators in many instances.[13] One group from MITLL used a commercial LiDAR tracking system with fairly fast acquisition to measure a 2.5m large inflatable optic, but this surface already had low reflectivity.[14] Finally, a group also created an inflatable membrane structure from mylar and used a method with laser scanning, but acquisition required many mechanical actuations.[15]

Seeking to obtain the similar measurement to that demonstrated by these groups, we contracted a printing company to print an evenly spaced 11 x 11 grid of diffuse red fiducial dots on the mylar mirror. In our LiDAR implementation, we used a laser distance meter aimed at precisely attitudes and azimuths to obtain the distance to each diffuse dot. We obtained a concave map as expected but noticed that measurements towards the aperture edge had a repeatability of 6 mm between acquisitions due to the weak return signal at oblique reflection angles.

We also used a 2-axis galvometer to steer a HeNe laser beam at same 121-point grid and captured the returning 'beam footprint' signal. Since system calibration data was known *a priori*¸ the footprint data could theoretically be input and optimized within Zemax OpticStudio to solve for the surface shape in regions where the beam was incident. In reality, up to 7 additional ghost images of the beam returned due to the interreflections between the two mylar membranes. Simple neutral density filters could remove dimmer ghosts and reduce the total number to 5. Alternatively, adding a polarizer in front of the camera reduced the number down to 1 – 3 because the metal/dielectric interreflections produce successively polarized beams, which can be distinguished. However, no single polarizer orientation could extinguish all ghost reflections across the full aperture. The combined effects of optical birefringence from the thickness variation at the transmissive front surface and polarization by reflection (based on angle of incidence) at the reflective back surface required at least four fast axis orientations to obtain the data for beam footprint analysis. Results yielded beam footprint sets that were indeed solvable by OpticStudio, but the hard-coded parameters were very sensitive and had to be recalibrated to adapt to small hardware position perturbations.

2.5 Photogrammetry Measurement of Low-Order Surface Figure

Photogrammetry experiments on the 1m mirror were promising. With a single camera capturing images of the UUT at two known positions, a point cloud fit well to the expected concave biconic surface, with a measurement repeatability up to 2 mm. An ideal photogrammetry configuration places two cameras at highly oblique angles from here, but here, available hardware limited that to less than 20 degrees and only 100 mm apart. Figure 5 shows the grid of dots, the image at a single camera position for centroiding and a resulting fitted surface. Engineering the system to achieve the 67 μm accuracy requirement is resource intensive due to the tradeoff between acquisition distance, camera position obliquity, and seen pixels per printed fiducial. At a higher cost for hardware, a photogrammetric solution could be produced to meet the requirements and therefore should not be ruled out.

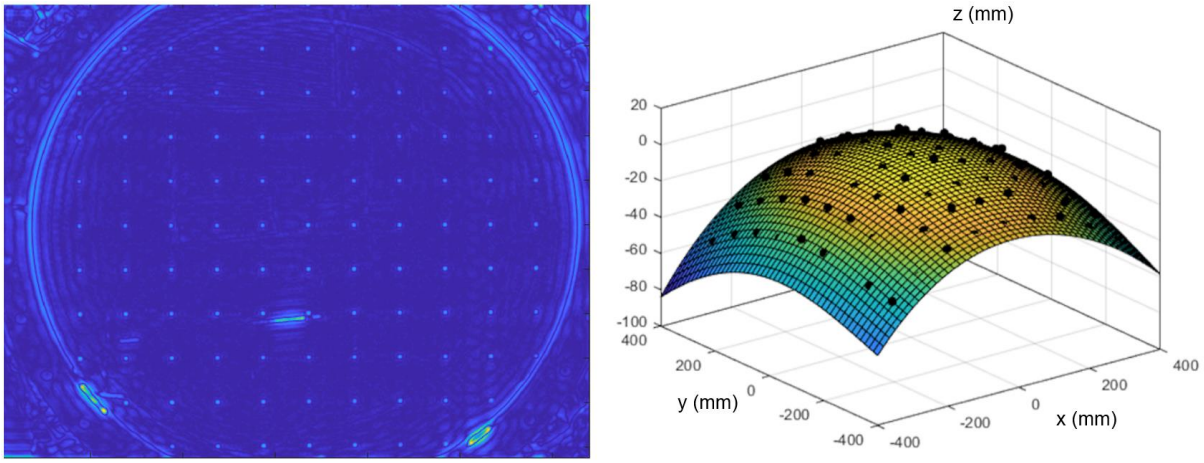

Figure 5. We used a Canon DSLR camera with ~6000 x 4000 pixels and low distortion 16 mm lens to capture movement of the fiducial centroids as the camera was translated. The subpixel positions of the fiducial centroids in the captured images are obtained using image processing software, where each dot was composed of ~20x20 pixels, a. Figure 5b shows our point cloud of acquired points from photogrammetry.

2.6 Deflectometry Measurement

At the moment, deflectometry piques substantial interest as the second metrology candidate. In contrast to interferometry, deflectometry (shown in Figure 6) is an incoherent measurement technique that relies on simple geometry, producing a large surface measurement range without requiring computer generated holograms (CGHs) or other nulling optics that are necessary to measure aspheres. The only hardware required is a configurable light source (typically a LCD display) and a camera to observe the reflection of the display through the UUT.

An ideal deflectometry configuration places the camera and illuminating source as close to the test optic's center of curvature (CoC) as physically possible. If the lateral distances between the hardware and the optical axis are small relative to their distance to the UUT, then the configuration minimizes the astigmatism arising from the off-axis imaging. Intuitively, this condition is easier to achieve with a further CoC since the lateral hardware distance is limited by the fixed dimensions of the camera body and the thickness of the illumination screen bezel.

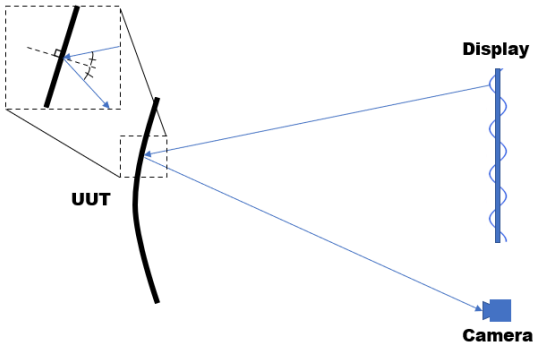

Figure 6. In phase-measuring deflectometry, a series of sinusoidal patterns from the display illuminate the UUT and encode an x-phase and y-phase at each pixel capturing the UUT image, as seen by the camera. Well-known unwrapping algorithms decode the wrapped phases at each pixel into an absolute x-phase and y-phase. These phases associate a physical coordinate at the LCD screen with each pixel of the UUT image. In this process, deflectometry associates a luminous sub-pixel screen location, a small discretized region at the UUT, and an illuminated pixel at the camera detector. Triangulating these three coordinates obtains a surface normal for each observed region of the UUT, which are converted to x and y slopes, and finally integrated to reconstruct the overall surface shape.[16,17]

Because deflectometry is fast, possesses high slope sensitivity, and can capture the full dynamic range of inflated concave shapes, our team heavily explored its applicability for measuring large membrane optics.

3. DEFLECTOMETRY EXPERIMENTS

3.1 Deflectometry Configuration for the 1m OASIS Prototype

When the membrane is inflated to 0.050 psig, a concave mirror with a CoC of approximately 4600 mm is produced. Similar to what is shown in Figures 7 and 8, a custom deflectometer using a 340 mm square computer monitor with 80 µm pitch and a PointGreyFL3-U3-13Y3M-C camera with a f = 25 mm lens captured the full x-slopes and y-slopes across the aperture. The screen and camera were set coplanar as to ease the simplicity of physical calibration. Here, the ratio of the lateral distance from the camera to the optical axis and the axial distance to the UUT aperture was ~75 mm / 4600 mm, which is approximately 0.02.

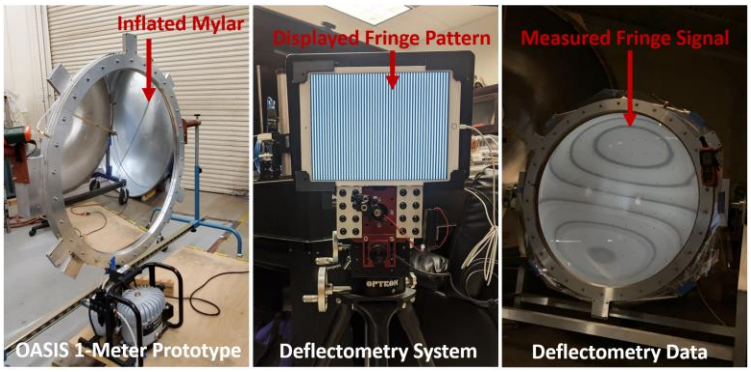

Figure 7. A different hardware setup was used for measurement than depicted, but this conceptually shows the configuration hardware. This system was specifically built so that it could be calibrated with a CMM, transported to the facility, and easily aligned with the in-situ mirror. The deflectometry assembly (LCD screen, laser, and camera) were affixed to an OPTRON telescope mount with 3 DOFs so alignment could be achieved between the mechanical axis of the mirror and the calibrated center point of the deflectometer.

For the UUT surface calibration, CMM-type equipment obtains physical points that help fit the design surface to the UUT's true physical coordinates. In the SCOTS (Software Configurable Optical Test System) implementation of deflectometry, it is assumed that the UUT true surface height is within microns of the design shape, as this is routinely achieved in optics shops.[18] For this peculiar optic, we simply sample the distance from the vertex to the tensioning ring base. Inflated membranes naturally follow a monotonic profile from aperture edge to the center, a truncated sphere is fit to the vertex

and known circular aperture edge coordinates. Overall, the slope error is low because even millimeters of deviation between the Hencky Surface and an approximate sphere is not direct surface error in the final surface reconstruction. The difference between the true surface shape and an approximate surface shape plays into slope calculation error, where slope at each surface point is calculated as $S_x = \Delta x / \Delta z$, where Δx is the lateral distance and Δz is the longitudinal distance relative to the optical axis. When Δz is around 4000 mm, a bilateral 1 mm uncertainty is insignificant towards the calculation of slope.

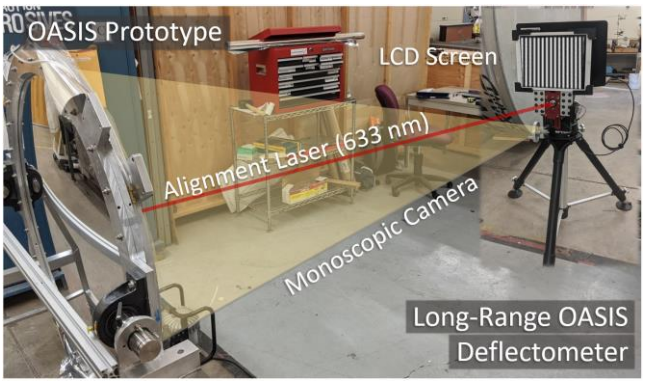

Figure 8. This is the conceptual testing configuration. The deflectometer was superimposed into picture because the 4000 mm longitudinal distance made the entire setup hard to capture within a single shot.

4. MEMBRANE MIRROR METROLOGY PERFORMANCE

4.1 Differential Deflectometry

A set of several deflectometry acquisitions at inflation pressures spanning from 0.040 psig to 0.080 psig were used to obtain different sag measurements, shown in Figure 9. The key idea is that calibration was static – all the hardware remained in place, including the camera, a different LCD screen, and fixed 1m membrane assembly. When slopes for the membrane at two pressures are obtained and subtracted, the error due to imprecise hardware calibration is removed because this error is identical between sets. Once the absolute slopes were subtracted, the slope difference was obtained and were integrated to obtain the surface height difference between pressures.

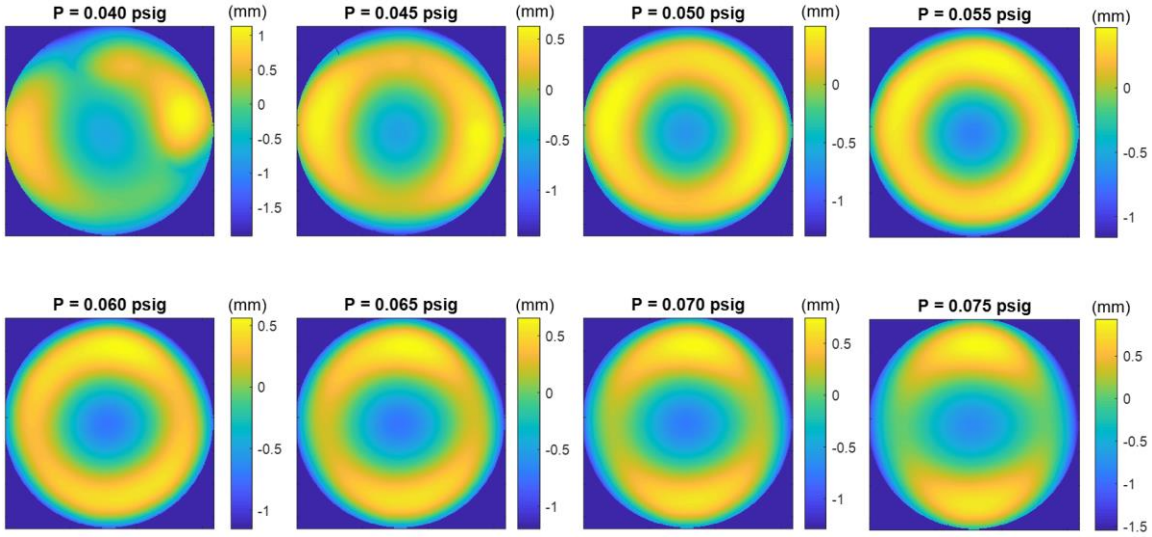

Figure 9. The shape of the optic at different pressures is observed from a top view of the full 1m circular aperture. The surface height maps are shown with Z1-Z4 removed. At lower pressures, stress is less evenly distributed across the aperture. Surface sag increases across the entire aperture with pressure but the successive sag gains level out at higher pressures. Note that the acquisition and full processing of these eight ~600 x 600 pixel maps took less than an hour total, after system calibration was established.

Reconstruction maps showed that each 0.005 psig increment increased the surface sag at the vertex by 1 mm, which matched contact-based measurements of the vertex displacement. Table 3 summarizes clear trends in the differential sag measurements in the form of Zernike decomposition.

Table 3. Zernike term decomposition of shape change between inflation pressures. In differential deflectometry measurements, trends in decomposed Zernike terms intuitively make sense. Sag change at the vertex was nearly exactly 0.97 mm between each 0.005 psig inflation, and the lower order power and astigmatism Zernike terms have nearly linear decreasing trendlines. Piston, coma, and foil changes of all orders were effectively nil. This suggests that the inflation pressure regime is within the elastic limits of the material.

		Inflation Pressure (psig)				
	Zernike Term	**0.055-0.060**	**0.060-0.065**	**0.065-0.070**	**0.070-0.075**	**0.075-0.080**
Z4	Defocus/Power (μm)	-280	-260	-254	-245	-214
Z5	Obliq. Astig. (μm)	0.41	-0.03	0.14	-0.13	-0.11
Z6	Vert. Astig. (μm)	-76.1	-69.6	-68.0	-67.4	-56.7
Z11	Spherical (μm)	-9.06	-8.41	-8.42	-8.37	-7.49
Z12	2nd Vert. Astig (μm)	0.91	0.81	0.50	0.55	0.53
Z13	2nd Obliq. Astig (μm)	-1.02	-0.79	-0.91	-0.88	-0.75

4.2 Absolute Deflectometry

For one instance of absolute deflectometry testing, we calibrated the entire system to within a certainty of 1 mm. Pressure was set to 0.050 psig, and the 'W-shaped' curve of past realized Hencky surfaces was observed when Z1-Z4 were removed, in Figure 10b.

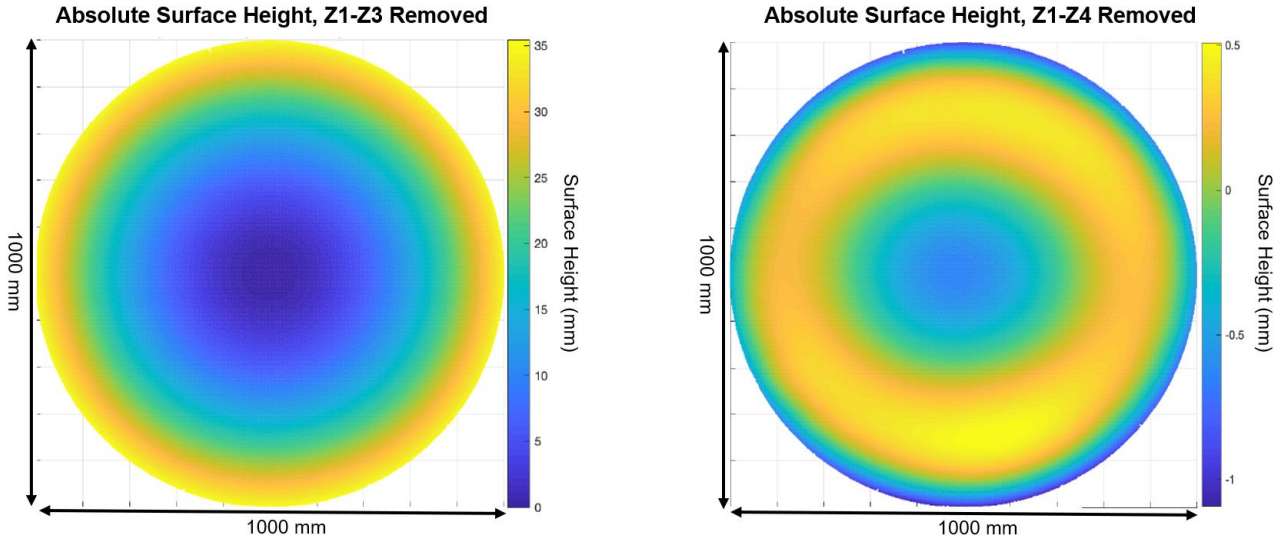

Figure 10. This is our absolute measurement map. The problem is here is that the predicted focal length from image conjugates was around 2300 mm, while the obtained surface from deflectometry has f_{medial} = 1768 mm and f_{RMS} = 1578 mm. Stopping down the aperture of the reconstructed surface had a negligible effective on medial focal length calculated by OpticStudio, although it increased the distance between sagittal and tangential focuses (1640 mm and 1537 mm respectively).

5. CONCLUSION AND FUTURE WORK

In light of COVID-19, we are unable to access the facility that houses the 1-m scale membrane model. Continuing interest in deflectometry and obtaining good agreement with the basic image conjugate testing motivated us to build a 6" mylar membrane model for continued testing and thermoforming process development, illustrated in Figure 11.

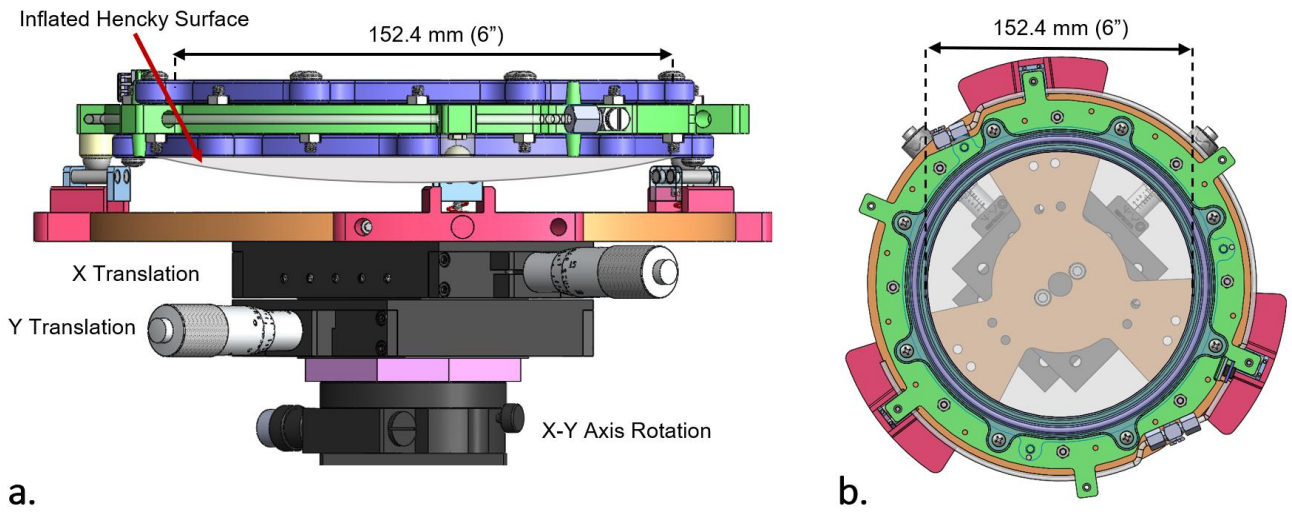

Figure 11. A profile view of the SolidWorks model is shown, a. Additional degrees of freedom for alignment are conferred by a rotation stage and two crossed linear stages. Kinematic mounting was implemented as three pairs of spheres (yellow) in double cylinder V-groove troughs (light blue). The inflated Hencky Surface protrudes from below the lower O-ring flange (lavender). An aerial view shows the aperture assembly as would be viewed by a camera in the deflectometry configuration, b. At this scale, the deflectometry test uses the iPad Pro LCD at 750 mm from the tensioning ring (green) and the same machine vision camera equipped with a f = 16 mm low-distortion lens.

Summarily, OASIS mission seeks to obtain high spectral resolution observations in the terahertz imaging regime. The membrane optic architecture possesses boasts vast light collecting ability and will advance our understanding of biogenic molecules in the formation and evolution of planetary systems. To assess applicable metrology techniques of the rear optical surface, we cast a wide net of techniques. Photogrammetry is one promising candidate that can sample the positions of the diffuse fiducials printed on the large concave mirror; a hardware solution that meets the 67 μm global accuracy requirement simply requires a larger investment of resources and a denser concentration fiducials. Deflectometry is the second promising candidate, which obtains dense measurement without fiducials; however, the focal lengths predicted by the global surface results remain to be reconciled with that determined by point-to-point conjugate imaging. Once back in the lab, the team suspects that both photogrammetry and well-calibrated deflectometry measurements will prove mutually reinforcing and could be used to cross-check the inflatable membrane shape across the full aperture.

ACKNOWLEDGEMENTS

The authors would like to acknowledge the II-VI Foundation Block-Gift, Technology Research Initiative Fund Optics/Imaging Program, and Friends of Tucson Optics Endowed Scholarships in Optical Sciences for helping support the metrology research conducted in the LOFT group.

REFERENCES

[1] Walker, C., Kulesa, C., Smith, I. S., Perry, W., Kim, D., Palisoc, A., Cassapakis, C., Crowe, D. and Pierce, D., "Orbiting Astronomical Satellite for Investigating Stellar Systems (OASIS)" (2019).
[2] Shapiro, I. I. and Jones, H. M., "Perturbations of the Orbit of the Echo Balloon," Science (80-.). **132**(3438), 1484–1486 (1960).
[3] Freeland, R. E. and Bilyeu, G., "IN-STEP INFLATABLE ANTENNA EXPERIMENT" (1993).
[4] Angel, J. R. P., Burge, J. H., Hege, E. K., Kenworthy, M. A. and Woolf, N. J., "Stretched membrane with electrostatic curvature (SMEC): a new technology for ultralightweight space telescopes," UV, Opt. IR Sp. Telesc. Instruments **4013**(July 2000), 699–705 (2000).
[5] Blonk, B. J. De, Moore, J. D., Patrick, B. G. and Flint, E. M., "Membrane Mirrors in Space Telescopes," Recent Adv. Gossamer Spacecr., 45–108 (2006).

[6] Atcheson, P., Domber, J., Whiteaker, K., Britten, J. A., Dixit, S. N. and Farmer, B., "MOIRE: ground demonstration of a large aperture diffractive transmissive telescope," Sp. Telesc. Instrum. 2014 Opt. Infrared, Millim. Wave **9143**(August 2014), 91431W (2014).
[7] Marker, D. and Jenkins, C., "Surface Precision of Optical Membranes with Curvature," Opt. Express **1**(11), 324 (1997).
[8] Hencky, H., "Über den Spannungszustand in kreisrunden Platten," Zeitschrift für Angew. Math. und Mech., 311–317 (1915).
[9] Meinel, A. B., "Inflatable membrane mirrors for optical passband imagery," Opt. Eng. **39**(2), 541 (2000).
[10] Finckenor, M. M. and Dooling, D., "Multilayer Insulation Material Guidelines," NASA Tech. Pap.(April 1999), 1–33 (1999).
[11] DuPont., "Mylar ® Product Information" (2003).
[12] Chandra, A. and Walker, C. K., "Thermally formed inflatable reflectors for space telescopes," IEEE(March) (2020).
[13] Arancibia-Bulnes, C. A., Peña-Cruz, M. I., Mutuberría, A., Díaz-Uribe, R. and Sánchez-González, M., "A survey of methods for the evaluation of reflective solar concentrator optics," Renew. Sustain. Energy Rev. **69**(December), 673–684 (2017).
[14] Mills, J. H., Fenn, A. J., Crowley, S., Hassan, B., Robey, F. C., Dufilie, P. and Hecht, M. H., "Space-Deployed Inflatable Dual-Reflector Antenna : Design and Prototype Measurements," 33rd Annu. AIAA/USU Conf. Small Satell.
[15] Patiño-Jiménez, F., Nahmad-Molinari, Y., Moreno-Oliva, V. I., De Los Santos-García, F. and Santiago-Alvarado, A., "Construction and optical testing of inflatable membrane mirror using structured light technique," Int. J. Photoenergy **2015** (2015).
[16] Faber, C., Olesch, E., Krobot, R. and Häusler, G., "Deflectometry challenges interferometry: the competition gets tougher!," Interferom. XVI Tech. Anal. **8493**(September 2012), 84930R (2012).
[17] Knauer, M. C., Kaminski, J. and Hausler, G., "Phase measuring deflectometry: a new approach to measure specular free-form surfaces," Opt. Metrol. Prod. Eng. **5457**(September 2004), 366 (2004).
[18] Su, P., Parks, R. E., Wang, L., Angel, R. P. and Burge, J. H., "Software configurable optical test system: a computerized reverse Hartmann test," Appl. Opt. **49**(23), 4404 (2010).